Research Square

Preprints are preliminary reports that have not undergone peer review.
They should not be considered conclusive, used to inform clinical practice,
or referenced by the media as validated information.

Hypoxia-Induced GP73 Promotes the Warburg Effect in Hepatocellular Carcinoma via HIF-1α

Mierkamilijiang Abudureheman
First Affiliated Hospital of Xinjiang Medical University
Diwen Zhu
First Affiliated Hospital of Xinjiang Medical University
Weixin Ren
rwx1031@163.com

First Affiliated Hospital of Xinjiang Medical University

Research Article

Keywords: Epithelial-mesenchymal transition, GP73, Hepatocellular carcinoma, Hypoxia-inducible factor-1α, Warburg effect

Posted Date: July 7th, 2026

DOI: https://doi.org/10.21203/rs.3.rs-10204910/v1

License: This work is licensed under a Creative Commons Attribution 4.0 International License.
Read Full License

Additional Declarations: No competing interests reported.

Version of Record: A version of this preprint was published at Molecular Biology Reports on October 22nd, 2026. See the published version at https://doi.org/10.1007/s11033-026-12991-5.

Abstract

Background

Hypoxia induced by transarterial chemoembolization (TACE) is a key driver of hepatocellular carcinoma (HCC) progression. This study investigated whether Golgi protein 73 (GP73) drives the Warburg effect and epithelial-mesenchymal transition (EMT) via hypoxia-inducible factor-1α (HIF-1α) under hypoxia, thereby promoting HCC malignancy.

Methods and Results

HepG2 cells were exposed to hypoxia (1% O_2). Lentivirus-mediated GP73 overexpression (LV-GP73) and siRNA-mediated HIF-1α knockdown (si-HIF-1α) were established. Four groups were compared: H + LV-NC (negative control), H + LV-GP73, H + LV-GP73 + si-NC, and H + LV-GP73 + si-HIF-1α. Cell proliferation, apoptosis, migration, and invasion were assessed by colony formation, flow cytometry, and Transwell assays. Glycolysis and mitochondrial respiration were evaluated by biochemical kits and Seahorse XFe24 Analyzer. Protein levels were detected by Western blotting. GP73 overexpression significantly enhanced colony formation, migration, invasion, glucose consumption, lactate production, LDH activity, ATP levels, and extracellular acidification rate, while decreasing apoptosis and oxygen consumption rate ($P < 0.05$), indicating Warburg effect activation. It also upregulated HIF-1α, glycolytic enzymes (HK2, SLC2A1, LDHA, PGK1), and Vimentin, but downregulated E-cadherin ($P < 0.05$). Notably, HIF-1α knockdown reversed all these pro-tumorigenic phenotypes, metabolic reprogramming, and molecular changes.

Conclusions

Under hypoxia, GP73 promotes the Warburg effect and EMT through HIF-1α stabilization, facilitating HCC progression. The GP73–HIF-1α axis is a critical mediator of TACE resistance and a potential therapeutic target.

Introduction

Hepatocellular carcinoma (HCC) is one of the most common malignancies worldwide and ranks as the second leading cause of cancer-related death in China, posing a serious threat to public health [1]. Transcatheter arterial chemoembolization (TACE) induces local ischemia and hypoxia by blocking the tumor blood supply while delivering chemotherapeutic agents locally, and has been recommended as the first-line therapy for intermediate-advanced HCC by multiple domestic and international guidelines [2], such as the Barcelona Clinic Liver Cancer (BCLC) staging system and the Guidelines for the Diagnosis and Treatment of Primary Liver Cancer (2024 Edition). In recent years, the application of drug-eluting beads, radioembolization microspheres, and “precision TACE” techniques has advanced the treatment;

however, the overall efficacy remains unsatisfactory—the 5-year survival rate is less than 20%, and recurrence and metastasis are the core causes of poor prognosis [3]. Therefore, identifying and targeting the key point of TACE treatment failure, namely “TACE resistance”, has become a research focus in interventional radiology.

Golgi glycoprotein 73 (GP73) is a 73-kDa type II Golgi transmembrane glycoprotein that was originally cloned from a patient with adult giant-cell hepatitis [4]. Large-scale international studies have shown that GP73 is highly expressed in HCC, and its diagnostic sensitivity and specificity are superior to those of alpha-fetoprotein (AFP)[5]. Investigations into the dynamic changes of GP73 before and after TACE have found that serum GP73 levels in HCC patients are significantly elevated at 1 day and 30 days post-TACE compared with pre-TACE levels, and that serum GP73 levels are positively correlated with the degree of tumor differentiation and BCLC stage[6]. These findings indicate that GP73 is not only a potential marker for the early diagnosis of HCC but may also participate in the TACE treatment response process.

Previous studies have demonstrated that GP73 can promote epithelial-mesenchymal transition (EMT) by enhancing the TGF-β/Smad signaling pathway [7]. Since EMT was first described in 1982, a large body of evidence has confirmed it as a key mechanism of tumor invasion and metastasis, in which the downregulation of E-cadherin and upregulation of Vimentin are regarded as hallmarks of EMT[8].

Hypoxia-inducible factor 1α (HIF-1α) plays a central transcriptional regulatory role in the hypoxic response [9]. Recent studies have shown that GP73 can competitively bind to prolyl hydroxylase 2 (PHD-2) in HCC cells, thereby inhibiting PHD-2-mediated hydroxylation and subsequent degradation of HIF-1α, stabilizing HIF-1α protein and promoting tumor angiogenesis [10]. This regulatory step is critical for tumor growth and metastasis.

Glycolysis is one of the key pathways for cellular energy supply [11]. In 1924, Otto Warburg first discovered that tumor cells preferentially utilize aerobic glycolysis rather than oxidative phosphorylation to meet their energy demands, even in the presence of ample oxygen—a phenomenon known as the “Warburg effect”[12]. Studies have indicated that, under hypoxic conditions, GP73 expression levels in HepG2 cells are strongly correlated with key glycolytic enzymes and related metabolites, suggesting that GP73 may mediate critical steps in glycolysis [13].

Taken together, we hypothesize that TACE resistance may be associated with GP73 stabilizing HIF-1α, which in turn drives the Warburg effect and EMT in HCC cells. This study aims to validate this hypothesis and explore the underlying mechanisms through in vitro experiments.

Materials and methods

Cell Culture and Hypoxic Treatment

The human hepatocellular carcinoma cell line HepG2 was purchased from Yaji Biological (Shanghai, China). Cells were cultured in MEM high-glucose medium (GIBCO, 41090-036) supplemented with 10%

fetal bovine serum (Excell Bio, FND500) and 1% penicillin–streptomycin solution (GIBCO, 15070-063), and maintained in a humidified incubator at 37°C with 5% CO_2. When cells reached 80%–90% confluence, they were dissociated with 0.25% trypsin-EDTA (GIBCO, 25200-056) for passaging. To simulate the hypoxic microenvironment, cells were placed in a tri-gas incubator and cultured under an atmosphere of 1% O_2, 5% CO_2, and 94% N_2 at 37°C with saturated humidity for 72 hours. All experiments were performed using cells in the logarithmic growth phase.

siRNA Transfection and qRT-PCR Analysis

Small interfering RNAs (siRNAs) targeting three independent sites of the HIF-1α gene (designated siRNA-HIF-1α-1, -2, and – 3) and a negative control siRNA (siRNA-NC) were synthesized by General Biol (Anhui, China). Transfection was performed using Lipofectamine™ RNAiMAX transfection reagent (Invitrogen™, 13778075) under optimized conditions determined in preliminary experiments, with a final siRNA concentration of 0.1 μM and a transfection duration of 48 hours. GP73-overexpressing lentivirus (LV-GP73) and the empty vector control lentivirus (LV-NC) were also constructed by General Biol, and cells were infected at an appropriate multiplicity of infection for 48 hours.

Total RNA was extracted from each group using TRIzol™ Reagent (Ambion, 15596026) according to the manufacturer's instructions. RNA purity was assessed with a microspectrophotometer (A260/A280 ratio, 1.8–2.1), and RNA integrity was confirmed by 1% agarose gel electrophoresis (showing clear 28S and 18S ribosomal RNA bands). One microgram of total RNA was reverse-transcribed into cDNA using the 5X All-In-One RT MasterMix (abm, G492). Quantitative real-time PCR (qRT-PCR) was performed on a Real-Time PCR System (K9600, Hangzhou Suizhen) using EvaGreen Express 2×qPCR MasterMix-Low Rox (abm, G891). The primer sequences were as follows: HIF-1α forward, CCACCTCTGGACTTGCCTTT, and reverse, GTGGCAACTGATGAGCAAGC; GP73 forward, TGGGCTTCAACTACTG, and reverse, TCTCCCTGGAACTCG; and β-actin (internal control) forward, GGACTTCGAGCAAGAGATGG, and reverse, AGCACTGTGTTGGCGTACAG. The thermal cycling protocol consisted of an initial denaturation at 95°C for 3 minutes, followed by 40 cycles of 95°C for 15 seconds and 60°C for 1 minute. Relative gene expression was calculated using the 2^−ΔΔCt method with β-actin as the endogenous control. All samples were run in triplicate.

Western Blot Analysis

Cells from each group were collected, washed twice with pre-chilled PBS, and lysed with RIPA lysis buffer containing protease inhibitors to extract total protein. Protein concentration was determined using a BCA assay. Equal amounts of protein (20–30 μg) were separated by SDS-polyacrylamide gel electrophoresis (SDS-PAGE) and transferred onto PVDF membranes. The membranes were blocked with 5% non-fat dry milk at room temperature for 1 hour and then incubated overnight at 4°C with the following primary antibodies: anti-HIF-1α (abcam, ab179483), anti-GP73 (Affinity, DF8100), anti-HK2 (CST, 2867S), anti-SLC2A1/GLUT1 (Proteintech, 21829-1-AP), anti-LDHA (CST, 3582S), anti-PGK1 (CST, 3248S), anti-E-

cadherin (Proteintech, 20874-1-AP), anti-Vimentin (CST, 5741S), and anti-β-actin (Sino Biological, 100166-MM10) as an internal control. The next day, after washing, the membranes were incubated with the corresponding HRP-conjugated secondary antibodies at room temperature for 1 hour. Following additional washes, protein bands were visualized using a chemiluminescence imaging system (Servicebio, SCG-W3000 PLUS). Band intensities were quantified using ImageJ software, and relative protein expression was expressed as the ratio of the target protein band intensity to that of β-actin. All experiments were independently repeated three times.

Experimental Groups

To investigate the effects of GP73 overexpression and HIF-1α knockdown on the biological behavior and metabolism of HepG2 cells under hypoxic conditions, the following four experimental groups were established: H + LV-NC group: Cells were infected with the empty vector control lentivirus (LV-NC) as a negative control and subsequently cultured under hypoxic conditions (1% O_2, 5% CO_2, 94% N_2) for 72 hours; H + LV-GP73 group: Cells were infected with the GP73-overexpressing lentivirus (LV-GP73) and cultured under the same hypoxic conditions for 72 hours; H + LV-GP73 + si-NC group: Cells were simultaneously infected with LV-GP73 lentivirus and transfected with the negative control siRNA (si-NC), followed by hypoxic culture for 72 hours. This group served to exclude potential non-specific effects of siRNA transfection; H + LV-GP73 + si-HIF-1α group: Cells were simultaneously infected with LV-GP73 lentivirus and transfected with siRNA targeting HIF-1α (si-HIF-1α), followed by hypoxic culture for 72 hours. This group was used to verify the critical role of HIF-1α in GP73-mediated effects.

Colony Formation Assay

HepG2 cells from each experimental group were collected and seeded into 12-well plates at a density of 500 cells per well, with three replicate wells per group. The cells were cultured in a humidified incubator at 37°C with 5% CO_2, and the complete culture medium was replaced every three days. After 9 days of culture, the medium was removed, and the cells were gently washed twice with PBS. The cells were then fixed with 4% formaldehyde at room temperature for 20 minutes. After removing the fixative, the cells were stained with 0.1% crystal violet solution at room temperature for 5 minutes. Following staining, the cells were washed twice with PBS and air-dried at room temperature. Colonies consisting of ≥ 50 cells were observed and photographed under a microscope, and the number of colonies was counted using ImageJ software. Colony formation was expressed as the number of colonies per well. The experiment was independently repeated three times.

Apoptosis Assay

HepG2 cells were treated according to the aforementioned experimental groups. After 72 hours of hypoxic culture, cells from each group were harvested. The culture supernatant, which contained floating apoptotic or necrotic cells, was transferred to a centrifuge tube. The adherent cells were washed twice

with PBS, and the washes were collected into the same tube. The adherent cells were then digested with 0.25% trypsin-EDTA; once the cells became rounded and began to detach, digestion was terminated by adding complete culture medium. The resulting cell suspension was collected into the centrifuge tube and centrifuged at 1,000 rpm for 5 minutes, after which the supernatant was discarded. The cell pellet was washed twice with pre-chilled PBS and centrifuged again, and the supernatant was carefully removed. The cells were resuspended in 500 μL of 1× Binding Buffer and filtered through a 200-mesh sieve to obtain a single-cell suspension. To each tube, 5 μL of Annexin V-PE and 10 μL of 7-AAD staining solution (BD, 559763) were added, gently mixed, and incubated at 4°C in the dark for 10 minutes. Stained samples were analyzed by flow cytometry (URIT, BF-700) within 30 minutes, and at least 1×10^4 cells were acquired per sample. The apoptosis rate was expressed as the sum of the percentages of early apoptotic cells and late apoptotic cells. Three replicate wells were set up for each group, and the experiment was independently repeated three times.

Cell Migration Assay

Cell migration was assessed using Transwell chambers (Corning, 3422). HepG2 cells from each experimental group described above were collected, washed once with PBS and once with serum-free MEM medium, and then resuspended in serum-free medium at a density of 2×10^5 cells/mL. In a 24-well plate, 600 μL of complete medium containing 10% FBS was added to the lower chamber as a chemoattractant. The Transwell inserts (upper chamber) were placed into the wells, and 100 μL of the cell suspension (i.e., 2×10^4 cells per well) was added to the upper chamber. Three replicate wells were set up for each group. The plate was incubated at 37°C in a 5% CO_2 incubator for 72 hours. After incubation, the inserts were carefully removed with forceps, washed twice with PBS, and fixed with 4% formaldehyde at room temperature for 20 minutes. Following fixation, the formaldehyde was discarded, and the inserts were washed twice with PBS. The inserts were then transferred into wells containing 600 μL of 0.1% crystal violet staining solution and stained at room temperature for 5 minutes. After staining, the inserts were rinsed twice with PBS, and non-migrated cells on the upper surface of the membrane were gently removed with a moistened cotton swab. The inserts were air-dried at room temperature with the lower surface facing upward. The migrated cells on the lower surface were observed and photographed under an optical microscope. Five random fields (200× magnification) were selected per insert to count the number of migrated cells, and the average was used to represent the number of migrated cells per well. The experiment was independently repeated three times.

Cell Invasion Assay

Matrigel (Corning, 356234) was thawed overnight at 4°C and diluted to 1 mg/mL with pre-chilled serum-free MEM medium. A 100 μL aliquot of the diluted Matrigel was added to the bottom of the upper chamber of each Transwell insert (Corning, 3422) and incubated at 37°C for 5 hours to allow gelation. HepG2 cells from each experimental group were collected, washed once with PBS and once with serum-free medium, and then resuspended in serum-free medium at a density of 2×10^5 cells/mL. Complete

medium (600 μL) containing 10% FBS was added to the lower chamber, and 100 μL of the cell suspension (2×10^4 cells per well) was added to the upper chamber. Three replicate wells were set up for each group. After incubation at 37°C in a 5% CO_2 incubator for 72 hours, the inserts were removed, washed with PBS, fixed with 4% formaldehyde for 20 minutes, and stained with 0.1% crystal violet for 5 minutes. Non-invaded cells and the Matrigel layer on the upper surface of the membrane were gently removed with a moistened cotton swab. After air-drying, the invaded cells on the lower surface were observed and photographed under an optical microscope. Five random fields (200× magnification) were selected per insert to count the number of invaded cells. The experiment was independently repeated three times.

Measurement of Metabolic Biochemical Parameters

HepG2 cells and culture supernatants from each experimental group were collected. The following parameters were measured according to the manufacturers' instructions: residual glucose in the supernatant was determined using a Glucose Assay Kit (Nanjing Jiancheng, A154-1-1); lactate levels in both the supernatant and cell lysates were measured using a Lactate Assay Kit (Nanjing Jiancheng, A019-2-1); lactate dehydrogenase (LDH) activity in the supernatant was assessed using an LDH Assay Kit (Nanjing Jiancheng, A020-2-2); and intracellular ATP levels were quantified using an ATP Assay Kit (Solarbio, BC0300). Lactate and ATP values obtained from cell lysates were normalized to total protein content and expressed per gram of protein (gprot). All procedures were performed in strict accordance with the kit instructions. Three replicate wells were set up for each group, and the experiment was independently repeated three times.

Seahorse Measurement of Oxygen Consumption Rate and Extracellular Acidification Rate

HepG2 cells treated as described in Section 2.4 were seeded into a Seahorse XFe24 cell culture plate (Agilent, 102342-100) at a density of 1×10^5 cells per well and cultured overnight. Prior to the assay, the culture medium was replaced with XF DMEM basal medium (Agilent, 103575-100). For OCR measurement, the medium was supplemented with 10 mmol/L glucose, 1 mmol/L pyruvate, and 2 mmol/L glutamine; for ECAR measurement, the medium was supplemented with 2 mmol/L glutamine. The sensor cartridge was hydrated overnight in a 37°C non-CO_2 incubator. Drugs were prepared and loaded into the cartridge according to the instructions of the Mitochondrial Stress Test Kit (Agilent, 103015-100) and the Glycolytic Stress Test Kit (Agilent, 103020-100). For the OCR assay, the following compounds were injected sequentially: oligomycin (1.5 μmol/L), FCCP (3 μmol/L), and rotenone/antimycin A (0.5 μmol/L). For the ECAR assay, the sequential injections were: glucose (10 mmol/L), oligomycin (1.0 μmol/L), and 2-deoxyglucose (50 mmol/L). OCR and ECAR values were measured and recorded using the XFe24 Analyzer. The experiment was independently repeated three times.

Western Blot Analysis

HepG2 cells from each experimental group described in Section 2.4 were collected, and total protein was extracted on ice using RIPA lysis buffer (Boster, AR0105) containing protease and phosphatase inhibitors. Protein concentration was determined using a BCA Protein Assay Kit (TransGen Biotech, DQ111-01). Equal amounts of protein (30 μg) were separated by SDS-PAGE and transferred onto PVDF membranes (Millipore, IPVH00010). The membranes were blocked with 5% non-fat milk at room temperature for 1 hour and then incubated overnight at 4°C with primary antibodies against HIF-1α, GP73, HK2, SLC2A1, LDHA, PGK1, E-cadherin, Vimentin, and β-actin as an internal control (all at dilutions ranging from 1:400 to 1:1000). The next day, the membranes were incubated with HRP-conjugated secondary antibodies (Abcam, 1:5000–1:10000) at room temperature for 1 hour. Protein bands were visualized using ECL chemiluminescence, and images were captured with a chemiluminescence imaging system. Band intensities were quantified using ImageJ software, and relative protein expression was expressed as the ratio of the target protein band intensity to that of β-actin. The experiment was independently repeated three times.

Statistical Analysis

All data are presented as mean ± standard deviation (SD). Statistical analyses were performed using SPSS 19.0 software. One-way analysis of variance (ANOVA) was used for group comparisons, and a P value < 0.05 was considered statistically significant. Graphs were generated using GraphPad Prism 5.0.

Results

Validation of HIF-1α Knockdown and GP73 Overexpression Cell Models

To determine the optimal siRNA transfection conditions, HepG2 cells were transfected with FAM-labeled negative control siRNA at different concentrations (0.01 μM and 0.1 μM) and cultured for 24 h and 48 h, respectively, before observation under a fluorescence microscope. The results showed that transfection with 0.1 μM for 48 h yielded the highest proportion of fluorescent-positive cells with well-maintained cell morphology (Fig. 1); therefore, this condition was adopted for all subsequent experiments.

The qRT-PCR results demonstrated that, compared with the Control group (1.002 ± 0.076) and the siRNA-NC group (1.002 ± 0.049), all three HIF-1α siRNA constructs significantly reduced HIF-1α mRNA levels, with siRNA-HIF-1α-1 achieving the highest knockdown efficiency (reduced to 0.355 ± 0.023, P < 0.05) (Fig. 2A). Western blot analysis further confirmed that HIF-1α protein expression was markedly decreased following siRNA-HIF-1α-1 transfection (from 0.392 to 0.211, P < 0.05) (Fig. 2B,C). Additionally, after infection with LV-GP73 lentivirus, GP73 mRNA levels increased from 1.002 ± 0.081 in the Control group and 1.000 ± 0.035 in the LV-NC group to 2.274 ± 0.047 (P < 0.05) (Fig. 2D). Western blotting also verified a significant elevation in GP73 protein levels (from 0.502 to 0.855, P < 0.05) (Fig. 2E,F). These findings indicate that the HIF-1α knockdown and GP73 overexpression cell models were successfully established, and siRNA-HIF-1α-1 along with LV-GP73 were selected for subsequent experiments.

GP73 Overexpression Promotes HepG2 Cell Proliferation and Inhibits Apoptosis via HIF-1α

The colony formation assay results showed that the number of colonies in the H + LV-GP73 group (175.667 ± 16.803) and the H + LV-GP73 + si-NC group (179.333 ± 3.055) was significantly increased compared with the H + LV-NC group (57.333 ± 3.215, $P < 0.05$), whereas the number of colonies in the H + LV-GP73 + si-HIF-1α group (82.333 ± 7.024) was markedly lower than that in the H + LV-GP73 group ($P < 0.05$) (Fig. 3A, C). Flow cytometric analysis of apoptosis revealed that the apoptosis rate was 20.237 ± 1.090% in the H + LV-NC group, which was significantly reduced in the H + LV-GP73 group (10.540 ± 1.063%) and the H + LV-GP73 + si-NC group (10.743 ± 0.764%, $P < 0.05$). In contrast, the apoptosis rate in the H + LV-GP73 + si-HIF-1α group (15.483 ± 0.569%) increased significantly compared with the GP73 overexpression group ($P < 0.05$) (Fig. 3B). These results indicate that GP73 overexpression significantly enhances the proliferative capacity of HepG2 cells and suppresses apoptosis, and that knockdown of HIF-1α partially reverses these effects.

GP73 Overexpression Promotes HepG2 Cell Migration and Invasion via HIF-1α

Transwell migration assay results showed that the numbers of migrated cells in the H + LV-GP73 group (380.667 ± 14.048) and the H + LV-GP73 + si-NC group (372.333 ± 9.074) were significantly increased compared with the H + LV-NC group (233.667 ± 14.295, $P < 0.05$), whereas the migratory capacity of the H + LV-GP73 + si-HIF-1α group (261.333 ± 9.504) was significantly decreased relative to the GP73 overexpression group ($P < 0.05$) (Fig. 4A, B). The invasion assay yielded similar results: the numbers of invaded cells in the H + LV-GP73 group (330.000 ± 15.716) and the H + LV-GP73 + si-NC group (334.000 ± 16.093) were significantly higher than that in the H + LV-NC group (169.333 ± 13.051, $P < 0.05$), while the invasive ability of the H + LV-GP73 + si-HIF-1α group (184.667 ± 7.234) was significantly reduced ($P < 0.05$) (Fig. 4A, B). These findings indicate that GP73 overexpression promotes the migration and invasion of HepG2 cells, and that this effect is dependent on HIF-1α.

GP73 Overexpression Drives the Warburg Effect via HIF-1α

To evaluate changes in glucose metabolism, residual glucose, lactate levels, and LDH activity in the culture supernatant, as well as intracellular lactate and ATP levels, were measured. Compared with the H + LV-NC group, the H + LV-GP73 group and the H + LV-GP73 + si-NC group exhibited increased glucose consumption (indicated by lower residual glucose), elevated lactate and LDH levels in the supernatant ($P < 0.05$), and significantly higher intracellular lactate and ATP levels ($P < 0.05$). In the H + LV-GP73 + si-HIF-1α group, however, these metabolic changes were significantly reversed: residual glucose increased, and lactate, LDH, and ATP levels fell back to near control levels (Fig. 5A, B). These data indicate that GP73 overexpression promotes aerobic glycolysis (the Warburg effect) in HepG2 cells, and that this effect is dependent on HIF-1α.

GP73 Overexpression Reprograms Energy Metabolism via HIF-1α (Seahorse Analysis)

The extracellular acidification rate (ECAR) and oxygen consumption rate (OCR) were measured using the Seahorse XFe24 Analyzer. The ECAR results demonstrated that, compared with the H + LV-NC group, both glycolysis and glycolytic capacity were significantly elevated in the H + LV-GP73 group ($P < 0.05$), whereas these parameters were significantly decreased in the H + LV-GP73 + si-HIF-1α group (Fig. 6A, B). The OCR results showed that basal respiration and maximal respiration tended to decrease in the GP73 overexpression group, though the differences did not reach statistical significance; however, both basal respiration and maximal respiration were significantly increased in the H + LV-GP73 + si-HIF-1α group compared with the GP73 overexpression group ($P < 0.05$) (Fig. 6C, D). These findings indicate that GP73 overexpression enhances glycolysis and suppresses mitochondrial respiration, and that knockdown of HIF-1α reverses this metabolic reprogramming.

GP73 Overexpression Upregulates Glycolysis- and EMT-Related Protein Expression via HIF-1α

Western blotting was performed to detect the expression levels of key glycolytic pathway proteins and EMT markers in each group. The results showed that, compared with the H + LV-NC group, the protein expression levels of HIF-1α, GP73, HK2, SLC2A1 (GLUT1), LDHA, PGK1, and the mesenchymal marker Vimentin were significantly upregulated in the H + LV-GP73 group and the H + LV-GP73 + si-NC group ($P < 0.05$), whereas the expression of the epithelial marker E-cadherin was significantly downregulated ($P < 0.05$). In the H + LV-GP73 + si-HIF-1α group, all of the above protein expression changes were significantly reversed: the expression of glycolytic enzymes and Vimentin decreased, while E-cadherin expression increased (Fig. 7A, B). These results confirm at the molecular level that GP73 overexpression upregulates key glycolytic enzymes and induces EMT via HIF-1α, thereby promoting the malignant phenotype of hepatocellular carcinoma cells.

Discussion

HCC is one of the most common malignancies worldwide[14]. Although TACE is the standard treatment for intermediate-advanced HCC, treatment failure and disease progression due to TACE resistance remain major clinical challenges[15]. GP73 has been established as a potential serum biomarker for HCC, and its expression level is closely correlated with tumor stage and patient prognosis[16]. However, the specific mechanism by which GP73 regulates tumor metabolic reprogramming under a hypoxic microenvironment has remained unclear [17]. The present study is the first to systematically demonstrate that, under hypoxic conditions, GP73 stabilizes and activates HIF-1α, thereby driving aerobic glycolysis and EMT, which in turn promote the proliferation, migration, and invasion of HCC cells while inhibiting apoptosis[10]. More importantly, rescue experiments with HIF-1α knockdown

significantly reversed all the pro-tumorigenic phenotypes and metabolic alterations induced by GP73 overexpression, confirming the central hub role of HIF-1α in the downstream signaling pathway of GP73.

In this study, we first successfully established HepG2 cell models with GP73 overexpression and HIF-1α knockdown. The results of qRT-PCR and Western blot validation showed that LV-GP73 lentiviral infection increased GP73 mRNA and protein levels by approximately 2.3-fold and 1.7-fold, respectively, whereas siRNA-HIF-1α-1 knocked down HIF-1α mRNA to approximately 35% of the control level, with a corresponding marked decrease in protein expression. These models provided a reliable foundation for subsequent functional and mechanistic studies.

At the cellular phenotypic level, our results are consistent with previous reports: GP73 overexpression significantly enhanced the colony-forming ability, migration, and invasion of HCC cells, while concurrently inhibiting apoptosis[18]. These data further support the notion that GP73 functions as an oncoprotein rather than merely a biomarker. Notably, all of the above phenotypic changes were significantly reversed upon HIF-1α knockdown, indicating that the tumor-promoting function of GP73 is highly dependent on HIF-1α. This finding is consistent with the previously reported mechanism by which GP73 competitively binds to prolyl hydroxylase 2, thereby inhibiting the hydroxylation-dependent degradation of HIF-1α[19].

The core novelty of this study lies in elucidating the function of GP73 from a metabolic perspective. Through biochemical assays and Seahorse real-time energy metabolism analysis, we systematically demonstrated for the first time that GP73 overexpression drives the Warburg effect in HCC cells: increased glucose consumption, elevated lactate production, enhanced LDH activity, elevated intracellular ATP levels, a marked increase in ECAR, and a decreasing trend in mitochondrial OCR. Knockdown of HIF-1α completely reversed these metabolic changes. These findings indicate that GP73, via HIF-1α, reprograms the energy metabolism of HCC cells from oxidative phosphorylation toward aerobic glycolysis, thereby providing a metabolic advantage for rapid tumor cell proliferation and survival [20].

At the molecular level, Western blot results revealed that GP73 overexpression upregulated HIF-1α protein levels and subsequently increased the expression of multiple key glycolytic enzymes, including glucose transporter GLUT1 (SLC2A1), HK2, LDHA, and PGK1. Concurrently, GP73 overexpression induced EMT, as evidenced by the downregulation of the epithelial marker E-cadherin and the upregulation of the mesenchymal marker Vimentin. Notably, HIF-1α knockdown not only reversed the expression of glycolytic enzymes but also restored E-cadherin expression and suppressed Vimentin. These results indicate that the GP73-HIF-1α axis simultaneously regulates metabolic reprogramming and cell motility, synergistically promoting the malignant progression of HCC[21].

The findings of this study have significant clinical translational implications. TACE induces local hypoxia by blocking the tumor blood supply, and hypoxia is a well-established stimulus for both HIF-1α stabilization and GP73 upregulation[22]. Clinical studies have reported that serum GP73 levels are significantly elevated in HCC patients after TACE, and that high GP73 levels are associated with poor tumor differentiation, advanced stage, and unfavorable prognosis[6]. Taken together with our in vitro

data, it is reasonable to hypothesize that the hypoxic microenvironment induced by TACE may upregulate the GP73→HIF-1α signaling axis, thereby activating the Warburg effect and EMT, endowing residual tumor cells with enhanced invasive capacity and metabolic adaptation, and ultimately promoting the development of TACE resistance[23]. Therefore, targeting GP73 or HIF-1α may represent a potential therapeutic strategy for overcoming TACE resistance[23]. For instance, the combination of HIF-1α inhibitors or glycolysis inhibitors with TACE may enhance therapeutic efficacy[24].

This study has several limitations. First, all experiments were performed exclusively in the HepG2 cell line, without validation in other HCC cell lines or primary hepatocytes; thus, the generalizability of the results requires further confirmation. Second, this study was conducted entirely in vitro and lacks validation in animal models in vivo (xenograft tumor models in nude mice and TACE simulation models). Future studies should establish stable cell lines with GP73 overexpression or knockout and evaluate their effects on tumor growth, metastasis, and TACE efficacy in vivo. Finally, the precise molecular mechanism by which GP73 regulates HIF-1α stabilization (whether through PHD2 interaction, deubiquitination, or other post-translational modifications) needs to be further elucidated by co-immunoprecipitation and ubiquitination assays.

Conclusion

This study aimed to elucidate, at the molecular level, the mechanisms underlying TACE resistance driven by the post-procedural hypoxic microenvironment, and to provide theoretical targets for the future development of molecular imaging probes (GP73-targeted PET/CT tracers) or TACE combined with targeted sensitization therapy. Our experiments demonstrated that, under hypoxic conditions, GP73 overexpression activates HIF-1α, thereby driving aerobic glycolysis and epithelial-mesenchymal transition in hepatocellular carcinoma cells, which in turn significantly enhances cell proliferation, migration, and invasion while inhibiting apoptosis. Knockdown of HIF-1α completely reversed the above effects, indicating that the function of GP73 is highly dependent on HIF-1α. This study is the first to systematically delineate the critical role of the “GP73–HIF-1α–Warburg effect/EMT” signaling axis in the malignant progression of HCC, and provides a theoretical basis for targeting this axis to overcome TACE resistance.

Declarations

Ethics Approval

This study used commercially available cell lines and did not involve human participants, animal subjects, or patient-derived tissues. Therefore, ethics approval was not required.

Competing Interests

The author(s) declared no potential conflicts of interest with respect to the research, authorship, and/or publication of this article.

Consent to Participate

Not applicable.

Consent for Publication

Not applicable.

Funding

This study was supported by the Tianshan Talents Program for Medical and Health High-Level Talents Training Plan of the Health Commission of Xinjiang Uygur Autonomous Region (Grant No. TSYC202301B032)

Author Contribution

M. and Z. conceived and designed the study. M. performed the experiments, analyzed the data, and drafted the manuscript. R. supervised the project, acquired funding, and revised the manuscript. All authors read and approved the final manuscript.

Data availability

The raw data supporting the conclusions of this article will be made available by the authors, without undue reservation.

References

1. Zheng S, Chan SW, Liu F, Liu J, Chow PKH, Toh HC, Hong W (2024) Hepatocellular carcinoma: current drug therapeutic status, advances and challenges. Cancers 16(8):1582. https://doi.org/10.3390/cancers16081582
2. Lv X, Ma M, Zhao Z, Li Y, Kong J, Shao G, Tang W, Xiong F (2026) Degradable multifunctional microspheres for combined thermotherapy-embolization-immune activation therapy of hepatocellular carcinoma. Adv Healthc Mater 15(10):e04261. https://doi.org/10.1002/adhm.202504261
3. Vulasala SSR, Sutphin PD, Kethu S, Onteddu NK, Kalva SP (2023) Interventional radiological therapies in colorectal hepatic metastases. Front Oncol 13:963966. https://doi.org/10.3389/fonc.2023.963966

4. Liu MY, Huang L, Wu JF, Zhang HB, Ai WB, Zhang RT (2022) Possible roles of Golgi protein-73 in liver diseases. Ann Hepatol 27(5):100720. https://doi.org/10.1016/j.aohep.2022.100720
5. Pang BY, Leng Y, Wang X, Wang YQ, Jiang LH (2023) A meta-analysis of clinical values of 11 blood biomarkers, such as AFP, DCP, and GP73 for diagnosis of hepatocellular carcinoma. Ann Med 55(1):42–61. https://doi.org/10.1080/07853890.2022.2153163
6. Yu WM, Li GW, Lou MG, Wu ZY (2023) A meta-analysis of the prognostic impact of tissue golgi protein 73 (tGP73) in hepatocellular carcinoma. BMC Gastroenterol 23(1):401. https://doi.org/10.1186/s12876-023-03050-5
7. Liu Y, Hu X, Liu S, Zhou S, Chen Z, Jin H (2021) Golgi phosphoprotein 73: the driver of epithelial-mesenchymal transition in cancer. Front Oncol 11:783860. https://doi.org/10.3389/fonc.2021.783860
8. Yang L, Li J, Zang G, Song S, Sun Z, Li X et al (2022) Pin1/YAP pathway mediates matrix stiffness-induced epithelial–mesenchymal transition driving cervical cancer metastasis via a non-Hippo mechanism. Bioeng Transl Med 8(1):e10375. https://doi.org/10.1002/btm2.10375
9. Ghafouri-Fard S, Hussen BM, Shoorei H, Abak A, Poornajaf Y, Taheri M, Samadian M (2023) Interactions between non-coding RNAs and HIF-1α in the context of cancer. Eur J Pharmacol 943:175535. https://doi.org/10.1016/j.ejphar.2023.175535
10. Liu Y, Hu X, Zhou S, Sun T, Shen F, Zeng L (2024) Golgi protein 73 promotes angiogenesis in hepatocellular carcinoma. Res (Wash D C) 7:0425. https://doi.org/10.34133/research.0425
11. Kierans SJ, Taylor CT (2024) Glycolysis: a multifaceted metabolic pathway and signaling hub. J Biol Chem 300(11):107906. https://doi.org/10.1016/j.jbc.2024.107906
12. Akter R, Awais M, Boopathi V, Ahn JC, Yang DC, Kang SC, Yang DU, Jung SK (2024) Inversion of the Warburg effect: unraveling the metabolic nexus between obesity and cancer. ACS Pharmacol Transl Sci 7(3):560–569. https://doi.org/10.1021/acsptsci.3c00301
13. Liu J, Feng C, Zhao R, Song H, Huang L, Jiang N, Yang X, Liu L, Duan C, Wan L, Gao Q, Sun L, Hou X, Liu M, Zhang Y, Zhang X, Zhang D, Wang Y, Li Y, Ma X et al (2025) GP73 reinforces cytotoxic T-cell function by regulating HIF-1α and increasing antitumor efficacy. J Immunother Cancer 13(1):e009265. https://doi.org/10.1136/jitc-2024-009265
14. Rizzo A, Ricci AD (2022) Challenges and future trends of hepatocellular carcinoma immunotherapy. Int J Mol Sci 23(19):11363. https://doi.org/10.3390/ijms231911363
15. Huang JZ, Li JD, Chen G, He RQ (2024) Identification of the key genes and mechanisms associated with transcatheter arterial chemoembolisation refractoriness in hepatocellular carcinoma. World J Clin Oncol 15(1):62–88. https://doi.org/10.5306/wjco.v15.i1.62
16. Loosen SH, Halpaap J, Labuhn S, Bednarsch J, Alizai PH, Roeth AA, Lang SA, Vucur M, Kather JN, Knoefel WT, Ulmer TF, Neumann UP, Roderburg C, Luedde T (2022) Golgi protein 73 (GP73) serum levels predict outcome after resection of biliary tract cancer. Cancers 14(18):4428. https://doi.org/10.3390/cancers14184428

17. Bayliss RJ, Parker AL (2025) GP73: the key to unlocking immunotherapies efficacy in solid tumors? J Immunother Cancer 13(5):e011989. https://doi.org/10.1136/jitc-2025-011989
18. Liu L, Huang Y, Fu Y, Rao J, Zeng F, Ji M, Xu X, Zhu J, Du W, Liu Z (2022) Hepatitis B virus promotes hepatocellular carcinoma development by activating GP73 to repress the innate immune response. Infect Agents Cancer 17(1):52. https://doi.org/10.1186/s13027-022-00462-y
19. Zhang Y, Ji JL, Yao DD, Zhou Y, Liu CC, Tang ZL, Xue JL, Liu BC, Li ZL, Ma RX (2026) Oxaloacetate restores HIF-1α-mediated mitochondrial homeostasis to counter tubulointerstitial injury in diabetic kidney disease. Diabetes Obes Metab 28(5):4216–4231. https://doi.org/10.1111/dom.70612
20. Liu X, Deng H, Tang J, Wang Z, Zhu C, Cai X, Rong F, Chen X, Sun X, Jia S, Ouyang G, Li W, Xiao W (2022) OTUB1 augments hypoxia signaling via its non-canonical ubiquitination inhibition of HIF-1α during hypoxia adaptation. Cell Death Dis 13(6):560. https://doi.org/10.1038/s41419-022-05008-z
21. Xu Y, Ren B, Wang M (2023) HIF-1α contributes to metastasis in choriocarcinoma by regulating DEC1 expression. Clin Transl Oncol 25(6):1641–1649. https://doi.org/10.1007/s12094-022-03055-8
22. Wu T, Yao Y, Sun R, Wang H, Zhang J, Yin X et al (2021) Arterial instillation of rapamycin in treatment of rabbit hepatic xenograft tumors and its effects on VEGF, iNOS, HIF-1α, Bcl-2, Bax expression and microvessel density. Sci Prog 104(3):368504211026417. https://doi.org/10.1177/00368504211026417
23. Li S, Liu Y, Liu X, Wang X, Li W, Song M, Fu N, Guo Y, Li Z, Zhang Q, Liang J, Wang L, Zhang B (2026) Targeting HIF as a promising approach to synergize with immune checkpoint inhibitors. Int J Cancer. https://doi.org/10.1002/ijc.70515(Epub ahead of print)
24. Kao TW, Bai GH, Wang TL, Shih IM, Chuang CM, Lo CL, Tsai MC, Chiu LY, Lin CC, Shen YA (2023) Novel cancer treatment paradigm targeting hypoxia-induced factor in conjunction with current therapies to overcome resistance. J Exp Clin Cancer Res 42(1):171. https://doi.org/10.1186/s13046-023-02724-y

Figures

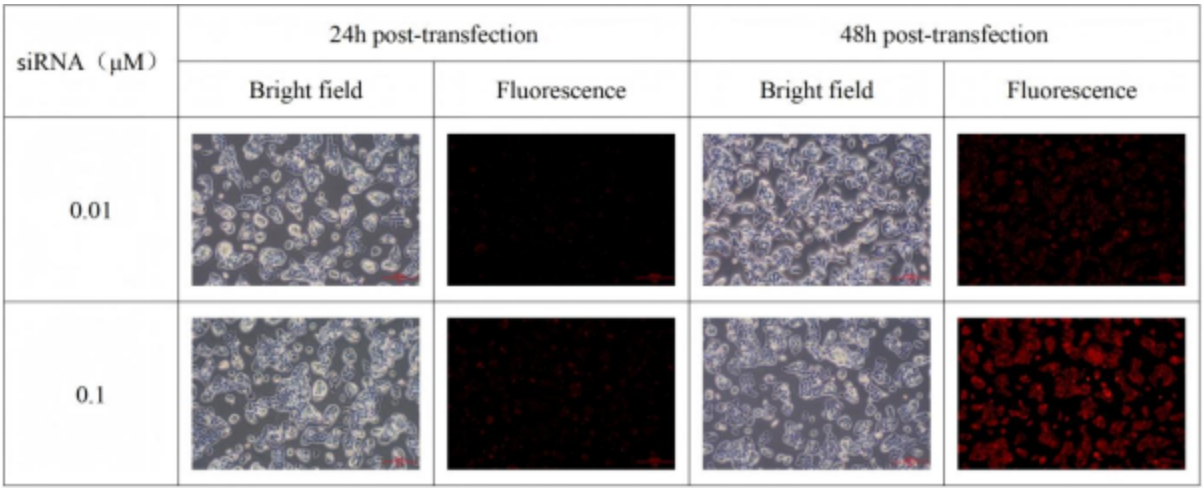


Figure 1

Optimization of siRNA transfection conditions in HepG2 cells. Cells were transfected with FAM-labeled negative control siRNA at different concentrations (0.01 μM and 0.1 μM) and cultured for 24 h or 48 h, then observed under a fluorescence microscope. The highest proportion of fluorescent-positive cells with well-maintained morphology was achieved at 0.1 μM for 48 h; thus, this condition was used for all subsequent experiments. For each group, bright-field (left) and fluorescence (right) images are shown. Scale bar: 100 μm.

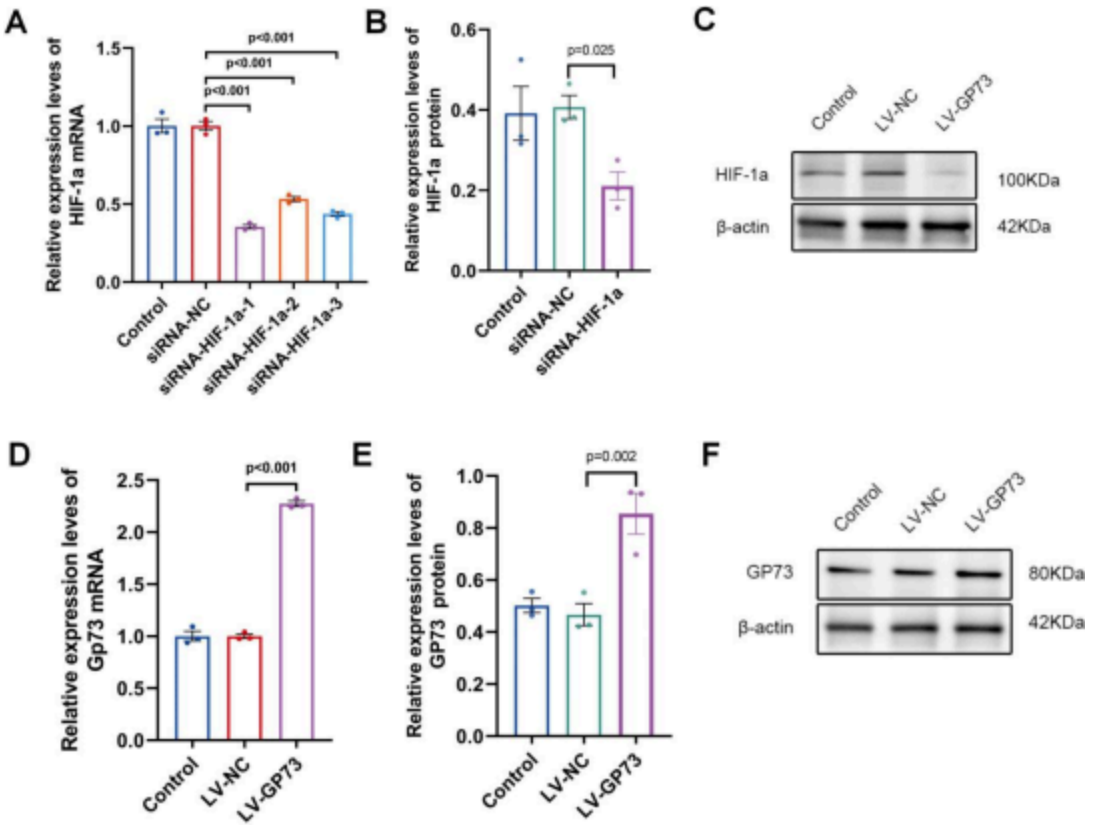


Figure 2

Validation of HIF-1α knockdown and GP73 overexpression in HepG2 cells. (A) qRT-PCR shows that siRNA-HIF-1α-1, -2, -3 all reduce HIF-1α mRNA levels; siRNA-HIF-1α-1 exhibits the highest knockdown efficiency (vs. Control or siRNA-NC, $p<0.001$). (B, C) Western blot confirms that HIF-1α protein expression is markedly decreased after siRNA-HIF-1α-1 transfection ($p<0.001$). (D) qRT-PCR shows that LV-GP73 infection significantly increases GP73 mRNA levels compared with Control and LV-NC groups ($p<0.001$). (E, F) Western blot confirms that GP73 protein expression is significantly elevated after LV-GP73 infection ($p<0.001$). Data are presented as mean±SD, n=3, one-way ANOVA.

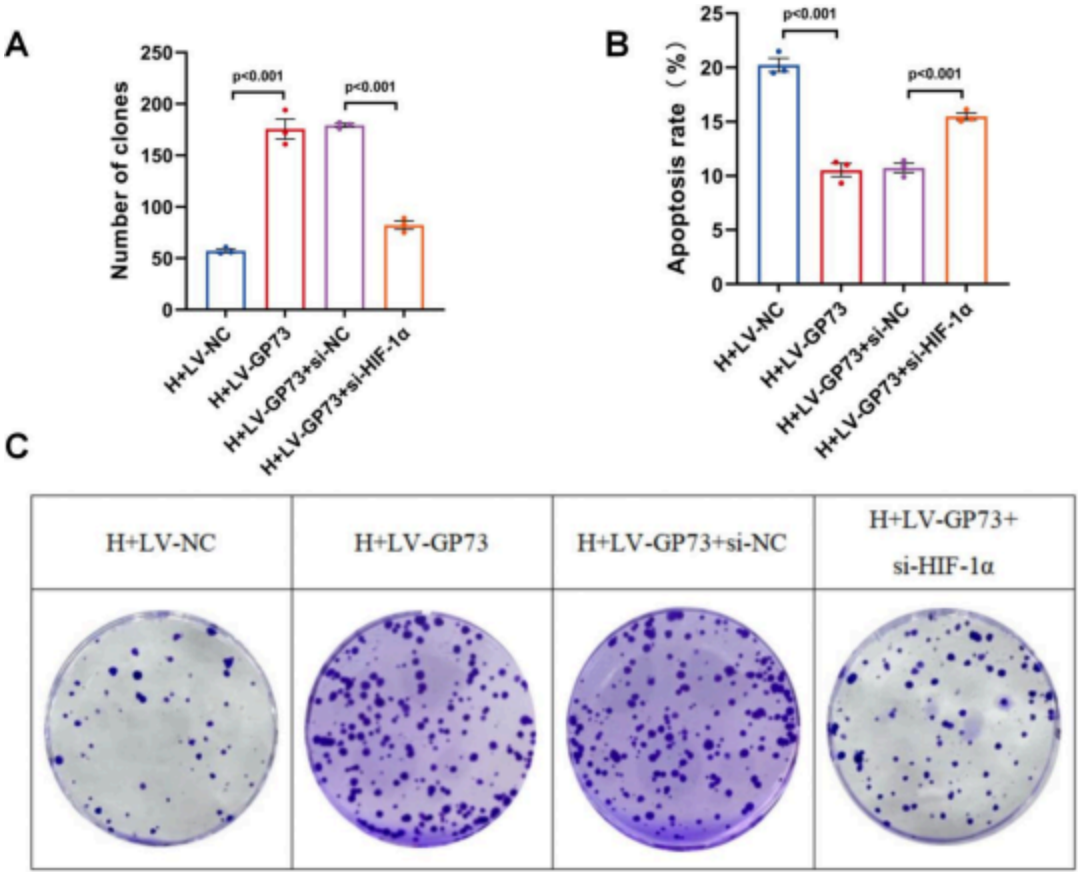


Figure 3

GP73 overexpression promotes proliferation and inhibits apoptosis in HepG2 cells via HIF-1α. (A) Quantification of colony formation. The number of colonies in the H+LV-GP73 group is significantly increased compared with the H+LV-NC group, and this effect is reversed by HIF-1α knockdown ($P<0.05$). (B) Apoptosis rate measured by flow cytometry. GP73 overexpression reduces apoptosis, whereas HIF-1α knockdown partially restores apoptosis ($P<0.05$). (C) Representative images of colony formation. Data are presented as mean±SD, n=3, one-way ANOVA.

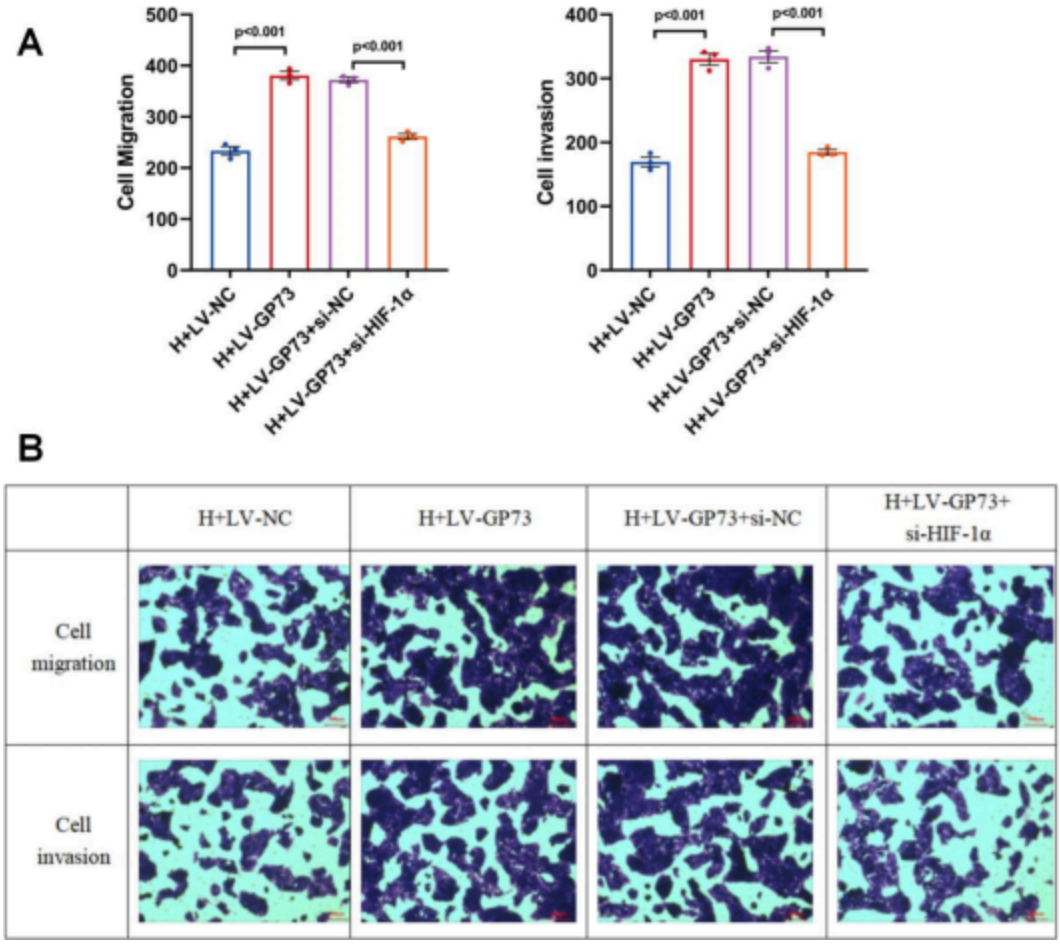


Figure 4

GP73 overexpression promotes migration and invasion of HepG2 cells via HIF-1α. (A) Quantification of migrated (left) and invaded (right) cells. Compared with the H+LV-NC group, the numbers of migrated and invaded cells are significantly increased in the H+LV-GP73 group, and these effects are reversed by HIF-1α knockdown (P<0.001). (B) Representative images of Transwell migration (upper panels) and invasion (lower panels) assays (crystal violet staining). Data are presented as mean±SD, n=3, one-way ANOVA. Scale bar: 100 μm.

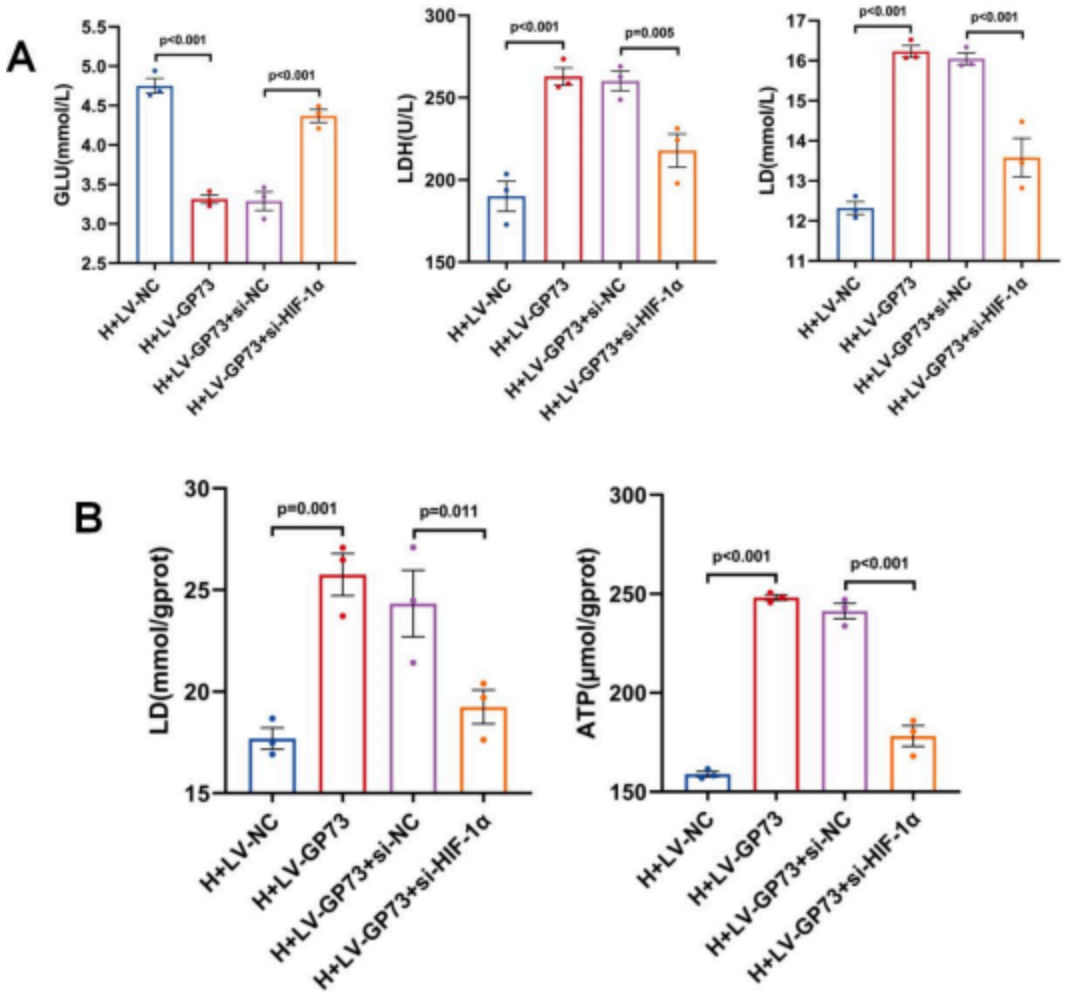


Figure 5

GP73 overexpression drives the Warburg effect in HepG2 cells via HIF-1α. (A) Residual glucose, lactate, and LDH activity in culture supernatant. Compared with the H+LV-NC group, the H+LV-GP73 group shows increased glucose consumption (decreased residual glucose), elevated lactate and LDH levels; these effects are reversed by HIF-1α knockdown (P<0.05). (B) Intracellular lactate and ATP levels. GP73 overexpression significantly increases both, whereas HIF-1α knockdown restores them to near control levels (P<0.05). Data are presented as mean±SD, n=3, one-way ANOVA.

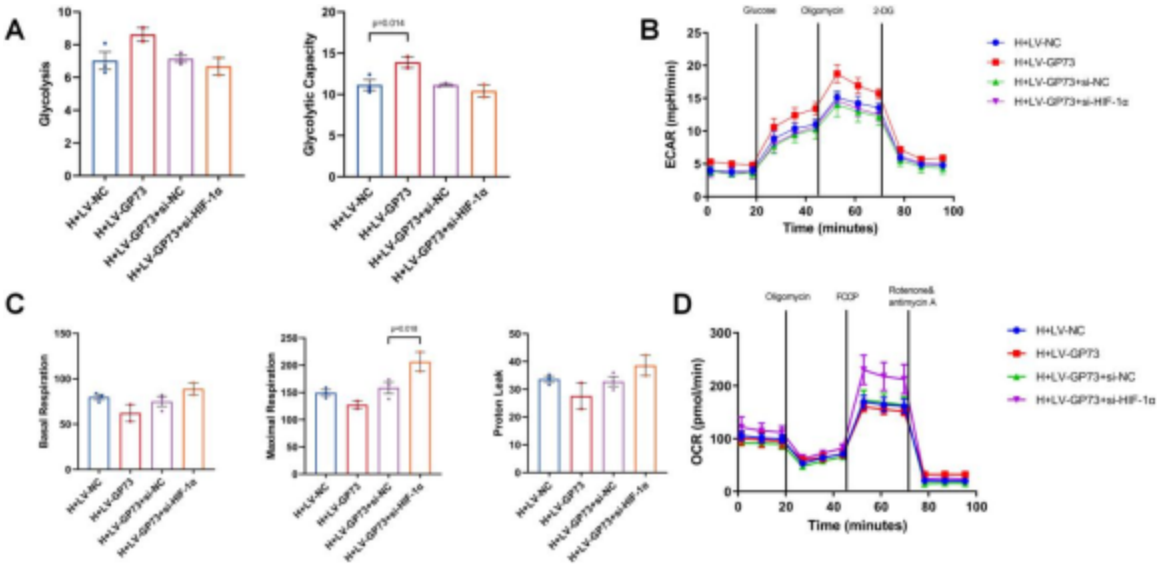


Figure 6

GP73 overexpression reprograms energy metabolism in HepG2 cells via HIF-1α. (A) Quantification of glycolysis and glycolytic capacity. Both parameters are significantly elevated in the H+LV-GP73 group compared with the H+LV-NC group, and decreased by HIF-1α knockdown (P<0.05). (B) Real-time ECAR profiles. (C) Quantification of basal respiration and maximal respiration. GP73 overexpression shows decreasing trends, whereas HIF-1α knockdown significantly restores both parameters (P<0.05). (D) Real-time OCR profiles. Data are presented as mean±SD, n=3, one-way ANOVA.

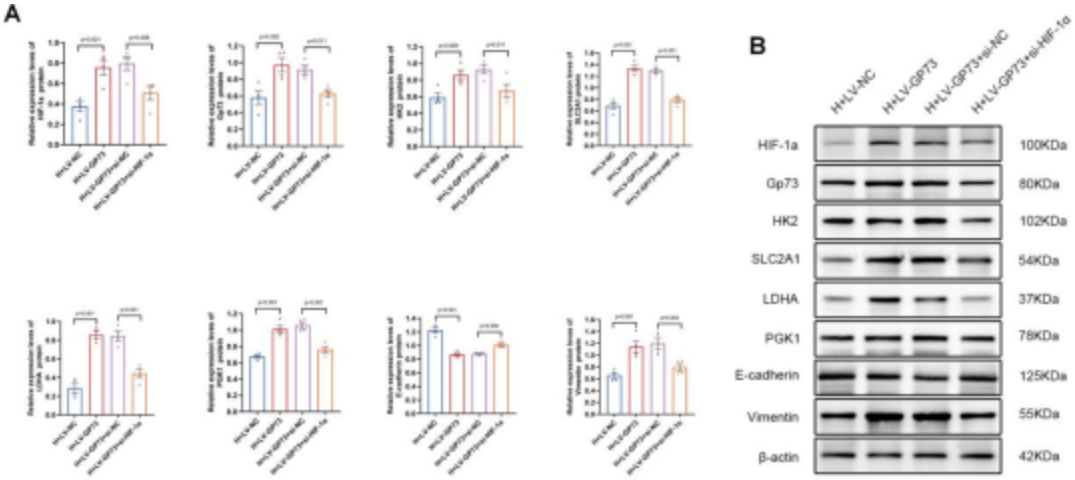


Figure 7

GP73 overexpression upregulates glycolytic key enzymes and induces EMT via HIF-1α. (A) Quantification of glycolytic proteins (HIF-1α, HK2, SLC2A1, LDHA, PGK1) and EMT markers (E-cadherin, Vimentin). Compared with the H+LV-NC group, GP73 overexpression significantly increases all above proteins except E-cadherin, which is decreased; these effects are reversed by HIF-1α knockdown (P<0.05). (B) Representative Western blot images. Data are presented as mean±SD, n=3, one-way ANOVA.